Atmos. Chem. Phys. Discuss., 9, 23791–23833, 2009
www.atmos-chem-phys-discuss.net/9/23791/2009/

Atmospheric Chemistry and Physics Discussions

This discussion paper is/has been under review for the journal Atmospheric Chemistry and Physics (ACP). Please refer to the corresponding final paper in ACP if available.

Impact of solar radiation on aerosol-cloud interactions in thin stratocumulus clouds

S. S. Lee and J. E. Penner

Department of Atmospheric, Oceanic, and Space Science, University of Michigan, Ann Arbor, MI, USA

Received: 2 September 2009 – Accepted: 29 September 2009 – Published: 11 November 2009

Correspondence to: S. S. Lee (seoungl@umich.edu)

Published by Copernicus Publications on behalf of the European Geosciences Union.

Abstract

This study examines the role of solar radiation in the effect of aerosols on liquid-water path (LWP) in thin, marine stratocumulus clouds with LWP of ~50 g m^{-2} or less by performing four sets of simulations with different solar radiation. Each set is composed of a simulation with present-day (PD) aerosols and a simulation with preindustrial (PI) aerosols. As solar radiation increases, decoupling within the marine boundary layer (MBL) becomes stronger, leading to less condensation and less LWP and thus the absence of the surface precipitation. This enables the evaporation of rain to affect the cloud-base instability. As rain evaporation increases due to more conversion of cloud liquid to rain in the PI case, the cloud-base instability increases and thus updrafts increase which leads to larger LWP in the PI case than in the PD case. In the cases with no surface precipitation, when solar radiation decreases and thus decoupling becomes weaker, rain evaporation and cloud-base instability become larger, which increases the LWP more with PI aerosols than with PD aerosols. As solar radiation decreases further, condensation and, thus, the LWP increase, which leads to the presence of the surface precipitation. This stabilizes the entire MBL and thus prevents the interactions that cause the evaporation of rain to enhance the cloud-base instability. In cases with the surface precipitation, the in-cloud interactions among cloud droplet number concentration (CDNC), supersaturation, and updrafts play an important role in the effect of aerosols on the LWP; these in-cloud interactions produce larger LWP with the PD aerosols than with the PI aerosols. In a case with lower solar radiation and with surface precipitation, weaker decoupling induces stronger in-cloud interactions, which results in larger increases in LWP with PD aerosols compared to PI aerosols than that in a case with higher solar radiation.

The results of this study demonstrate that solar radiation can act as an important environmental factor by inducing a large variation in the LWP and by changing the sign of aerosol effects on the LWP of thin stratocumulus clouds. Hence, the effect of solar radiation on decoupling and thus on the feedbacks between microphysics and

ACPD

9, 23791–23833, 2009

dynamics needs to be included in climate models for a better prediction of the effect of aerosols on clouds and thus climate.

1 Introduction

Aerosols act as cloud condensation nuclei (CCN) and thus affect cloud properties. Increasing aerosols are known to decrease droplet size and thus increase cloud albedo (the first aerosol indirect effect, AIE) (Twomey, 1974, 1977). They may also suppress precipitation and, hence, alter cloud mass and lifetime (the second AIE) (Albrecht, 1989). A significant effort has been directed towards gaining an understanding of the effect of aerosols on clouds, since this effect has been considered to be critical for the correct assessment of climate changes induced by human activities (Penner et al., 2001).

Lee et al. (2009) examined aerosol-cloud interactions in thin stratocumulus clouds with LWP of $\sim 50\,\mathrm{g\,m^{-2}}$ or less and with very small surface precipitation of $\sim 0.01\,\mathrm{mm\,day^{-1}}$ or less. A budget analysis of droplets (also referred to as cloud liquid in this study), showed that the conversion of droplets to rain via autoconversion (i.e. the growth of droplets to rain by collisions and condensation) and the accretion of droplets by rain were negligible in these thin clouds as compared to condensation. The terminal fall velocity of cloud particles to which the sedimentation rate is proportional increases with their increasing size. Also, the sedimentation of cloud mass is mainly controlled by the sedimentation of cloud particles larger than the critical size for active collection around ~20–~40 μm in radius (Pruppacher and Klett, 1997). Autoconversion and accretion are processes that control the growth of cloud particles after they reached the critical size or larger (Rogers and Yau, 1989). Hence, the small contribution of autoconversion and accretion to the cloud-liquid budget led to inactive sedimentation (resulting in the very small surface precipitation). Also, Lee et al. (2009) found that the change in conversion and sedimentation due to the change in aerosols from their PI level to PD level was negligible as compared to that of condensation in thin clouds. In other

ACPD
9, 23791–23833, 2009

words, it is the response of condensation to aerosols that mainly controls the response of cloud mass to aerosols, not that of the response of conversion and sedimentation. This is contrary to the traditional understanding of the second AIE which suggests that aerosols primarily affect cloud mass by changing the conversion of droplets to rain.

As shown in Lee et al. (2009), the response of condensation to aerosols is controlled by the aerosol-induced variation of interactions between microphysics and dynamics in thin stratocumulus clouds. Since it is well-known that dynamics in stratocumulus clouds is closely linked to the decoupling of the MBL, solar radiation, which controls the decoupling, is likely to affect the variation of interactions between microphysics and dynamics and thus the response of cloud mass to aerosols in thin clouds.

This study aims to examine how solar radiation affects aerosol-cloud interactions in thin clouds by varying the level of solar radiation. Several idealized cases of thin clouds are simulated with differences only in the level of solar radiation to better isolate the effect of solar radiation on these interactions.

2 Cloud-System Resolving Model (CSRM)

Here, the Goddard Cumulus Ensemble (GCE) model (Tao et al., 2003) is used as a CSRM, which is a three-dimensional nonhydrostatic compressible model. The detailed equations of the dynamical core of the GCE model are described by Tao and Simpson (1993) and Simpson and Tao (1993).

To represent microphysical processes, the GCE model adopts the double-moment bulk representation of Saleeby and Cotton (2004). Full stochastic collection solutions for self-collection among cloud droplets and for rain drop collection of cloud droplets based on Feingold et al. (1988) are obtained. The philosophy of bin representation of collection is adopted for the calculations of the drop sedimentation. The cloud droplet nucleation parameterization of Abdul-Razzak and Ghan (2000, 2002), which is based on the Köhler theory, is used. The change in the mass of droplets from vapor diffusion

ACPD
9, 23791–23833, 2009

(i.e. condensation and evaporation) is calculated by taking into account the predicted supersaturation and cloud droplet number concentration (CDNC).

The detailed description of the model used here can be found in Lee et al. (2009).

3 Case description

A case of thin marine stratocumulus located at (42° N, 60° W) off the coast of Maine is simulated here. Henceforth, this case is referred to as "CONTROL". A pair of 13-h simulations from 1 LST (local solar time) on 1 July to 14 LST on 1 July in 2002 are performed in which the aerosol concentration is varied from the PI level to the PD level. The simulation with the PD (PI) level is referred to as the high-aerosol (low-aerosol) run, henceforth. The PD and PI aerosols were those predicted using the CAM-IMPACT model.

The reanalysis data from the European Centre for Medium-Range Weather Forecasts (ECMWF) provided the initial conditions and large-scale forcings for the simulation. The 6-hourly analyses were interpolated to determine the large-scale advection of potential temperature and specific humidity at every time step. Temperature and humidity were nudged toward the large-scale fields from the ECMWF using this large-scale advection. The horizontally averaged wind from the GCE model was also nudged toward the interpolated wind field from ECMWF at every time step with a relaxation time of one hour, following Xu et al. (2002). The model domain is considered to be small compared to large-scale disturbances. Hence, the large-scale advection is approximated to be uniform over the model domain and large-scale terms are defined to be functions of height and time only, following Krueger et al. (1999). Identical observed surface fluxes of heat and moisture were prescribed in both the high- and low-aerosol runs. This method of modeling cloud systems was used for the CSRM comparison study by Xu et al. (2002). The details of the procedure for applying the large-scale forcings are described in Donner et al. (1999) and are similar to the method proposed by Grabowski et al. (1996).

ACPD
9, 23791–23833, 2009

Vertical profiles of initial specific humidity, potential temperature, and horizontal wind velocity applied to CONTROL can be seen in Fig. 1. The vertical distribution of the time- and area-averaged large-scale forcings of temperature and humidity imposed on CONTROL are depicted in Fig. 2. The profiles of humidity and potential temperature indicate that the initial inversion layer is formed around 400 m. Below the inversion layer, humidity, potential temperature, u (wind in the east-west direction) and v (wind in the north-south direction) velocities do not vary much. The positive values indicate eastward (northward) wind in u (v) velocities. The large-scale forcing of temperature decreases with height, while that of humidity decreases up to ~0.8 km and then increases.

Background aerosol data for the high-aerosol run and the low-aerosol run are provided by the CAM-IMPACT model during the simulation period. Aerosol data produced by the CAM-IMPACT model at (42° N, 60° W) from the PD and PI emissions are used for the high-aerosol run and low-aerosol run, respectively. The predicted aerosol mass of each aerosol species by the CAM-IMPACT model is obtained every 6 h. These mass data are interpolated into every time step to update the background aerosols. The aerosol mass is approximated to be uniform over the model horizontal domain and is defined to be a function of height and time only as are the large-scale forcings of temperature and humidity. The detailed description of the CAM-IMPACT model and aerosol emissions can be found in Wang et al. (2009). Aerosol number concentration is calculated from the mass profiles using parameters (mode radius, standard deviation, and partitioning of sulfate among modes) described in Chuang et al. (1997) for sulfate aerosols and Liu et al. (2005) for non-sulfate aerosols as in the CAM-IMPACT model. In the MBL, background aerosol number is nearly constant and only varies vertically within 10% of its value at the surface. The averaged aerosol number over the MBL is 700 (400) cm^{-3} for the high-aerosol (low-aerosol) run in the MBL. Assumptions for the aerosols follow those adopted in Lee et al. (2009) (see Sect. 4 in Lee et al. (2009) for the details of these assumptions).

ACPD
9, 23791–23833, 2009

The CSRM runs are performed in a 3-D framework. A uniform grid length of 50 m is used in the horizontal domain and the vertical grid length is uniformly 20 m below 3 km and then stretches to 480 m near the model top. Periodic boundary conditions are set on horizontal boundaries. The horizontal domain length is set to 12 km in both the east-west and north-south directions in this study to capture variations in mesoscale structures. The vertical domain length is 20 km to cover troposphere and the lower stratosphere.

4 Idealized cases

To isolate the dependence of the effect of solar radiation on the impact of aerosols on cloud mass, the simulations in CONTROL are repeated with differences only in downward solar radiation incident on the model top for radiation. There are additional layers only for radiation above 20 km (see Tao et al. (2003) for details of these layers) and the model top for radiation is at 0.01 hPa. For the first of these idealized cases, the top downward solar (or shortwave) radiation flux (SW) in CONTROL, multiplied by one and a half, is applied. This idealized case is referred to as "SW-M1.5". For the other idealized cases, the CONTROL-top SW which is divided (in the manner as shown in Table 1 which summarizes the simulations in this study) is applied. These idealized cases with the reduced model-top SW are named as shown in Table 1. Table 1 also shows the time- and area-averaged SW at the model top for radiation over the period with SW>0. Since the sun rises at 04:30 LST, the results among the cases are identical before 04:30 LST.

ACPD
9, 23791–23833, 2009

5 Results

5.1 Cloud properties

5.1.1 CONTROL

Figure 3 depicts the time-height cross section of cloud-liquid mixing ratio for the high-aerosol run (with the PD aerosol) and low-aerosol run (with the PI aerosol) from 30 min after the cloud formation to the end of simulation; in this paper, all the figures, depicting the time evolution of any variables, are over the period from 30 min after the cloud formation to the end of simulation. Figure 3 indicates that the maximum cloud depth is ~300 m in CONTROL. Except for the first and the last 30 min of the cloud evolution, the cloud fraction is larger than 0.8. Hence, shallow clouds with no substantial breakup are formed in CONTROL. In CONTROL, there is no surface precipitation for both the high- and low-aerosol runs.

Figure 4 depicts the temporal evolution of the domain-averaged LWP. Figure 4 shows that LWP in the high-aerosol run is higher than that in the low-aerosol run prior to ~05:30 LST in CONTROL. However, the LWP for low aerosols starts to be larger than that for high aerosols around ~05:30 LST, leading to a larger time- and domain-averaged LWP at low aerosol than at high aerosol; the time- and domain-averaged LWPs over the entire simulation period are 13.4 (17.1) $\mathrm{g\,m^{-2}}$ at high (low) aerosol in CONTROL (Table 2).

The simulated LWP in the high-aerosol run is compared to observations by the Moderate Resolution Imaging Spectroradiometer (MODIS) to assess the ability of the model to simulate stratiform clouds. The difference between the domain-averaged LWP in the high-aerosol run and the MODIS-observed LWP is less than 10% relative to LWP observed by the MODIS. This demonstrates that the LWP is simulated reasonably well. Figure 5 shows the vertical profile of the time- and domain-averaged simulated potential temperature and water-vapor mixing ratio in the high-aerosol run for CONTROL. The vertical coordinate is in the units of the height normalized with respect to the cloud-top

ACPD
9, 23791–23833, 2009

height (z_t). Triangles (Squares) in Fig. 5 are the retrieved potential temperature (water-vapor mixing ratio) from the MODIS observation at the MODIS-observation levels. Figure 5 demonstrates that the simulated potential temperature and humidity are also in good agreement with the MODIS observations.

5.1.2 Idealized cases

As in CONTROL, shallow clouds with no substantial break-up are formed in all of the idealized cases (Fig. 3).

The LWPs in the high-aerosol run and the low-aerosol run in SW-M1.5 are smaller than those in the high-aerosol run and the low-aerosol run in CONTROL (Fig. 4 and Table 2). Also, the LWP in the low-aerosol run starts to be larger than that in the high-aerosol run around 05:30 LST in SW-M1.5. This leads to a larger time- and domain-averaged LWP in the low-aerosol run than that in the high aerosol run as in CONTROL but with smaller differences in the LWP between the high- and low-aerosol runs (Fig. 4 and Table 2). Also, no precipitation reaches the surface in the high- and the low-aerosol runs in SW-M1.5 as is the case in CONTROL. However, the LWP is larger in the high-aerosol run than in the low-aerosol run in the other idealized cases (with the lower SW) throughout the simulation period (Fig. 4). Moreover, the difference in the LWP between the high-aerosol run and the low-aerosol run is larger in SW-D5 than in SW-D2.

In all of the cases, the LWP is around or smaller than $50\,g\,m^{-2}$ for the entire time integration and the time- and domain-averaged LWP is smaller than $50\,g\,m^{-2}$ (Fig. 4 and Table 2). Hence, according to the classification of Turner et al. (2007), clouds in all cases can be considered thin.

Due to the larger LWP, the low-aerosol case reflects more solar radiation than the high-aerosol case in SW-M1.5 and CONTROL by 1% and 3%, respectively, despite a smaller particle size in the high-aerosol case (Table 2). The percentage difference in the reflection of solar radiation between the high- and low-aerosol cases is larger in SW-D2 and SW-D5 than in SW-M1.5 and CONTROL, though the larger LWP contributes to larger reflection of solar radiation in the high-aerosol case than in the

ACPD
9, 23791–23833, 2009

low-aerosol case in SW-D2 and SW-D5. Because of both the increased LWP and the decreased particle size in the high-aerosol case, the difference in the reflection of solar radiation between the high- and low-aerosol cases is larger in SW-D2 and SW-D5 than in SW-1.5 and CONTROL. In SW-D2 and SW-D5, the high-aerosol case reflects 7 and 21% more solar radiation than the low-aerosol case, respectively.

5.2 Liquid-water budget and sedimentation

To elucidate the microphysical processes that control the liquid-water content (LWC) and thereby the LWP and their differences between the high-aerosol run and the low-aerosol run for each of the cases, the domain-averaged cumulative source (i.e. condensation) and sinks of cloud liquid and their differences between the high- and low-aerosol runs (high aerosol – low aerosol) were obtained. For this, the production equation for cloud liquid is integrated over the domain and the duration of the simulations. Integrations over the domain and duration of simulation are denoted by <>:

$$<A>=\frac{1}{LxLy}\iiint \rho_a A dx dy dz dt \quad (1)$$

where Lx and Ly are the domain length (12 km), in the east-west and north-south directions, respectively. ρ_a is the air density and A represents any of the variables in this study. The budget equation for cloud liquid is as follows:

$$<\frac{\partial q_c}{\partial t}>=<Q_{\text{cond}}>-<Q_{\text{evap}}>-<Q_{\text{auto}}>-<Q_{\text{accr}}> \quad (2)$$

Here, q_c is cloud-liquid mixing ratio. Q_{cond}, Q_{evap}, Q_{auto}, and Q_{accr} refer to the rates of condensation, evaporation, autoconversion of cloud liquid to rain, and accretion of cloud liquid by rain, respectively.

Table 2 shows the budget terms of Eq. (2). The budget shows that condensation and evaporation are ~1 to 2 orders of magnitude larger than the conversion of cloud liquid to rain (i.e. autoconversion + accretion of cloud liquid by rain); note that, as shown in Lee

et al. (2009), evaporation is controlled by condensation, since increasing (decreasing) condensation provides an increased (decreased) source of evaporation, leading to an increased (decreased) evaporation budget term. This indicates that the conversion of cloud liquid (produced by condensation) to rain is highly inefficient.

Autoconversion and accretion are processes that control the growth of cloud particles after they reached the critical size for active collections and the terminal fall velocity of cloud particles to which the sedimentation rate is proportional increases with their increasing size (Rogers and Yau, 1989). Hence, the small contribution of autoconversion and accretion to the LWC budget implies that the role of sedimentation of cloud particles in the determination of the LWC is not as significant as that of condensation.

Much larger differences in condensation as compared to those in the conversion of cloud liquid to rain between the high- and low-aerosol runs are simulated here (Table 2). This implies that changes in condensation (which control the changes in evaporation) due to aerosol increases play much more important roles in the LWP responses to aerosols than those in sedimentation.

Table 2 shows the domain-averaged cumulative cloud-mass changes due to in-cloud sedimentation for the high- and low-aerosol runs; here, the absolute value of the in-cloud sedimentation-induced mass change is presented. Cloud mass here is the sum of the mass of all species associated with warm microphysics, i.e. cloud liquid and rain. The magnitude of the condensation-induced change is substantially larger than that of the sedimentation-induced cloud-mass change in both high- and low-aerosol runs for all of the cases (Table 2). Also, the magnitude of a difference in condensation between the high- and low-aerosol runs is much larger than that in sedimentation-induced mass changes (Table 2). Hence, as implied by the budget analysis, the LWC and LWP and their responses to aerosols are mainly determined by condensation (controlling evaporation and its response to aerosols) and the role of sedimentation in their determination is not important.

5.3 Factors controlling condensation

5.3.1 SW-D2 and SW-D5

Here, an analysis of condensation, which plays the most important role in the LWP and its response to aerosols among the budget terms, is performed for SW-D2 and SW-D5.

The mass change of droplets from vapor diffusion, integrated over the size distribution, is given by:

$$\frac{d\overline{m}}{dt} = N_d 4\pi\psi F_{\mathrm{Re}} S \rho_{\mathrm{vsh}} \tag{3}$$

where N_d is CDNC, ψ vapor diffusivity, and ρ_{vsh} saturation water vapor mixing ratio. S is the supersaturation, given by $\left(\frac{\rho_{\mathrm{va}}}{\rho_{\mathrm{vsh}}} - 1\right)$ where ρ_{va} is water vapor mixing ratio. F_{Re} is the integrated product of the ventilation coefficient and droplet diameter which is given by

$$F_{\mathrm{Re}} = \int_0^\infty D f_{\mathrm{Re}} f_{\mathrm{gam}}(D) dD \tag{4}$$

where D is the diameter of droplets, f_{Re} the ventilation coefficient, and $f_{\mathrm{gam}}(D)$ the distribution function, given by $\frac{1}{\Gamma(\upsilon)}\left(\frac{D}{D_n}\right)^{\nu-1}\frac{1}{D_n}\exp\left(-\frac{D}{D_n}\right)$. f_{Re} is given by $\left[1.0+0.229\left(\frac{v_t D}{V_k}\right)^{0.5}\right]\eta$ where $v_t$is the terminal velocity and V_k the kinematic viscosity of air and η the shape parameter (Cotton et al., 1982).

Among the variables associated with the condensational growth of droplets in Eq. (3), differences in the supersaturation and the CDNC contribute most to the differences in condensation between the high- and low-aerosol runs. The percentage difference in the other variables is ~2 orders of magnitude smaller than those in supersaturation and CDNC throughout the simulations. Figure 6 shows the time series of CDNC and Fig. 7

the time series of supersaturation, conditionally averaged over areas where the condensation rate >0, for SW-D2 and SW-D5. Figures 6 and 7 indicate that supersaturation is generally larger at low aerosol than at high aerosol. However, the condensation rate is generally higher, leading to a larger cumulative condensation at high aerosol than at low aerosol in SW-D2 and SW-D5 as shown in Fig. 8. Figures 8c and d depict the time series of the domain-averaged cumulative condensation for these two cases. The larger condensation at high aerosol is ascribed to the larger CDNC providing a larger surface area for water-vapor condensation at high aerosol compared to that at low aerosol. The effects of the CDNC increase on the surface area of droplets and thus condensation compete with the effects of the supersaturation decrease on the condensation with increasing aerosols. This leads to a smaller condensation difference than the differences in CDNC and supesaturation. The effects of the increased surface area for condensation outweigh the effects of decreased supersaturation, leading to a larger cumulative condensation in the high aerosol runs in SW-D2 and SW-D5.

Increased condensation provides more condensational heating, which intensifies updrafts as shown in Fig. 9 which depicts the time series of the domain-averaged updraft mass flux for SW-D2 and SW-D5. Increased updrafts in turn increase condensation, establishing a positive feedback between updrafts and condensation. Therefore, the larger number of cloud droplets provide more surface area for condensation and thus induce stronger updrafts which plays a critical role in the increased condensation in cases where the LWP is higher at high aerosol. Note that increased condensation not only increases evaporation, and thus, entrainment, but also increases the LWC. In the cases where the LWP is higher for the high aerosol case, the effects of condensation on the LWC outweigh those of evaporation and entrainment, leading to an increase in the LWP for the high aerosol case. The interactions among CDNC, condensation and dynamics (i.e. updrafts) in these cases mainly determine the differences in condensation and thereby the LWP response to aerosols between the high- and low-aerosol runs.

5.3.2 SW-M1.5 and CONTROL

The intensified interactions between condensation and updrafts due to increased CDNC in SW-M1.5 and CONTROL lead to larger condensation and, thereby, LWP in the high-aerosol run than in the low-aerosol run prior to ~05:30 LST by compensating for the lower supersaturation (Fig. 4). The domain-averaged LWPs are 14.2 (12.5) and 13.1 (11.7) g m^{-2} in the high- and low-aerosol runs, respectively, prior to 05:30 LST in CONTROL (SW-M1.5). However, Fig. 8 shows that condensation rate (indicated by the slope of the cumulative condensation) begins to rapidly increase around 04:00 LST in CONTROL and SW-M1.5 in the low-aerosol case. As a result, the cumulative condensation becomes larger in the low-aerosol case than that in the high-aerosol case around 05:00 LST in both SW-M1.5 and CONTROL. This leads to a larger averaged LWP over the entire domain and simulation period in the low aerosol case than in the high aerosol case in SW-M1.5 and CONTROL. This indicates that there is a mechanism compensating for the decreased interactions among CDNC, condensation, and dynamics in the low-aerosol case in SW-M1.5 and CONTROL.

Surface precipitation is absent in SW-M1.5 and CONTROL. As indicated by Jiang et al. (2002), when precipitating particles evaporate completely before reaching the surface, even a slight increase in evaporation of precipitation around the cloud base can cause an increased instability concentrated around the cloud base. When precipitation reaches the surface, the associated cooling tends to stabilize the entire layer below the cloud (Paluch and Lenschow, 1991). Updrafts and downdrafts in the cloud and sub-cloud layers increase when precipitation does not reach the surface, since its evaporation increases instability around the cloud base (Feingold et al., 1996).

Figures 10a and 10b depict the vertical distribution of the domain-averaged rain evaporation in SW-M1.5 and CONTROL and confirm that precipitation does not reach the surface and that rain evaporates mostly around cloud base (at z/z_t~0.4) in both the high- and low-aerosol runs. Increased aerosols in the high-aerosol run delays the formation of precipitation, leading to smaller precipitation and thus its evaporation

around cloud base. As shown in Fig. 11a and b, depicting the vertical profile of the time- and domain-averaged rate of conversion of cloud liquid to rain in SW-M1.5 and CONTROL, more droplets are converted to rain in the low aerosol case. The time- and domain-averaged effective diameter of cloud droplets is 14 and 12 μm for the low and high aerosol cases, respectively. Larger particle size favors more efficient collisions among droplets and rain leading to a higher conversion of droplets to rain. Hence, more rain precipitates to around the cloud base at low aerosol than at high aerosol. This in turn leads to larger evaporation of rain just below the cloud base as shown in Fig. 10a and b. Figure 12a and b depict the domain-averaged profile of the lapse rate ($\frac{d\theta}{dz}$) over 04:00–05:00 LST in SW-M1.5 and CONTROL, and show that the increase in evaporation below cloud base leads to a larger instability in the low aerosol case prior to 05:00 LST ($\frac{d\theta}{dz}$ is smaller for the low aerosol case below cloud base). Here, θ is the potential temperature. Figures 13a and 13b show the domain-averaged profile of potential temperature over 04:00–05:00 LST. Smaller $\frac{d\theta}{dz}$ below cloud base leads to lower potential temperature in the low aerosol case around cloud base. This larger instability makes the variance of the vertical velocity at low aerosol larger than that at high aerosol after 04:00 LST as seen in a comparison between Fig. 14a (c) and b (d) in CONTROL (SW-M1.5). Stronger vertical motions lead to the rapidly increasing condensation around 04:00 LST and then to the larger cumulative condensation around 05:00 LST at low aerosol than at high aerosol in SW-M1.5 and CONTROL (Fig. 8).

The effect of aerosols on the instability around cloud base in SW-M1.5 and CONTROL competes with the interactions among CDNC, condensation, and dynamics; increased aerosols not only decrease the instability around cloud base but also increase interactions among CDNC, condensation and dynamics. The effects of decreased instability outweigh those of the intensified interactions with increased aerosols, leading to a smaller LWP in the high-aerosol run than in the low-aerosol run. However, the LWP increase at low aerosol is larger in CONTROL than in SW-M1.5. Due to smaller condensation, the available liquid water for the conversion of cloud liquid to rain becomes smaller in the low-aerosol case in SW-M1.5 as compared to that in the

ACPD
9, 23791–23833, 2009

low-aerosol case in CONTROL (see the smaller condensation in Table 2 in SW1.5 than in CONTROL). In addition to the smaller available liquid water, the conversion efficiency (i.e. the ratio between the conversion of cloud liquid to rain through autoconversion and accretion of rain by cloud liquid and condensation) is lower at low aerosol in SW-M1.5 than in CONTROL (Table 2). Small cloud droplets grow to a critical size for (active) collection not only by the turbulent collisions among them but also by condensation; for particles smaller than the critical size, condensational growth is as important as the growth through the turbulent collisions, and particles grow via positive feedbacks between the condensational growth and the growth through these turbulent collisions, though, above the critical size, the growth through collection is dominant (Rogers and Yau, 1991). Thus, as condensation decreases, these feedbacks get weaker and thus the conversion efficiency decreases as shown in Lee and Penner (2009). This leads to a reduced increase of precipitation supply to the cloud base and thus to a reduced increase of the cloud-base evaporative cooling at low aerosol in SW-M1.5 as compared to CONTROL as shown in Fig. 10. Hence, the increased cloud-base instability due to the increased rain evaporation at low aerosol in SW-M1.5 is not as large as that in CONTROL. This leads to a smaller increase in LWP at low aerosol in SW-M1.5 than that in CONTROL.

5.3.3 Role of solar radiation

While there is some surface precipitation in SW-D2 and SW-D5, rain does not reach the surface in SW-M1.5 and CONTROL (enabling the interactions between rain evaporation and cloud-base instability). This is mainly due to smaller conversion of cloud liquid to rain in SW-M1.5 and CONTROL than in SW-D2 and SW-D5 as shown in Fig. 11. Due to smaller condensation shown in Table 2, the liquid water available for the conversion of cloud liquid to rain is smaller in SW-M1.5 and CONTROL as compared to that in SW-D2 and SW-D5. In addition to the smaller available liquid water, the conversion efficiency is lower in SW-M1.5 and CONTROL due to the smaller condensation (Table 2), leading to weaker feedbacks between condensational growth and turbulent collisions

below the critical size for active collection. This leads to a lower sedimentation of rain and, thus, the amount of precipitating rain is not large enough to survive evaporation during its descent to the surface in SW-M1.5 and CONTROL (Fig. 10). The sub-cloud humidity can also acts as a factor in determining the presence of surface precipitation. However, the averaged differences in the sub-cloud relative humidity among the cases are within 10% of each other. Hence, it is unlikely that differences in the sub-cloud humidity play a role that is as important as differences in conversion and sedimentation in determining the presence or absence of the surface precipitation.

Figure 15 shows the vertical distribution of averaged buoyancy flux after sunrise. As shown there, the decoupling between the sub-cloud layer and the cloud layer is larger in SW-M1.5 and CONTROL than it is in SW-D2 and SW-D5. The buoyancy integral ratio (BIR) is ~0.14 and 0.12 in SW-M1.5 and CONTROL, while it is only ~0.02 and 0.01 in SW-D2 and SW-D5. The BIR is defined as the ratio of integral of magnitude of buoyancy fluxes over the regions of negative buoyancy below cloud-base to integral of buoyancy fluxes over all other regions (see Bretherton and Wyant, 1997, for more details of BIR). Larger BIR indicates more decoupling. After sunrise, the cloud layer is warmed more by solar radiation in SW-M1.5 and CONTROL than in SW-D2 and SW-D5. This leads to the larger negative sub-cloud buoyancy fluxes in SW-M1.5 and CONTROL as shown in Fig. 15, indicating that the turbulent circulations and associated mixing throughout the MBL are not as efficient as those in SW-D2 and SW-D5. Because the vertical mixing is stronger, the water vapor from the surface is more efficiently transported to the upper levels where it induces more condensation in SW-D2 and SW-D5 (leading to the presence of the surface precipitation) (Table 2).

We note that less warming of the cloud layer by solar radiation after sunrise occurs in CONTROL compared to that in SW-M1.5. This leads to a smaller negative buoyancy in sub-cloud layer as shown in Fig. 15, enabling more efficient mixing in the MBL in CONTROL than in SW-M1.5. With this more efficient mixing and thus more efficient transportation of the water vapor to upper levels, condensation in the low aerosol case in CONTROL is larger than that in SW-M1.5 at the initial stage of cloud development.

As explained in the previous section, this leads to more rain and larger cloud-base instability for the low aerosol case in CONTROL than in SW-M1.5.

Between the two cases with the surface precipitation, the increase in LWP for the high aerosol case is larger in SW-D5 than that in SW-D2. This indicates that the intensification of the interactions among CDNC, supersaturation, and updrafts with increasing aerosols increases with decreasing solar radiation. As shown in Fig. 15, there is a smaller decoupling in SW-D5 than in SW-D2. With smaller decoupling, the transport of water vapor is more efficient and this increases condensation more in SW-D5 than in SW-D2 (Table 2). Condensation in the high- and low-aerosol runs in SW-D5 increases as compared to that in the high- and low-aerosol runs in SW-D2. However, this condensation increase is larger between the high-aerosol runs than between the low-aerosol runs (leading to the larger increase in the LWP at high aerosol in SW-D5 than in SW-D2). The reason for this difference is that there is a ~50% increase in CDNC and a ~17% decrease in supersaturation in SW-D5, while there is a ~35% increase in CDNC and a ~23% decrease in supersaturation in SW-D2 in the high-aerosol case due to the increase in aerosols. This indicates that the smaller decoupling and the associated increase in the vertical transport of water vapor induces an increase in the number of nucleated droplets and a smaller decrease in the available water vapor for condensation at high aerosol in SW-D5 than that in SW-D2. Increased droplets tend to increase the competition among particles for available water vapor for condensation and this decreases supersaturation. However, despite the increase in droplets, the decrease in supersaturation is smaller at high aerosol in SW-D5 than at high aerosol in SW-D2. This indicates that there is a sufficiently increased supply of water vapor from the surface to counterbalance the effect of increasing CDNC on supersaturation in SW-D5 with its smaller decoupling. Figures 16a and b show that, around sunrise, the sub-cloud water-vapor flux is larger in the high-aerosol case than in the low-aerosol case in both SW-D5 and SW-D2 between 04:00 and 07:30 LST. Also, the difference in the sub-cloud water vapor flux between the high-aerosol run and the low-aerosol run in SW-D5 is similar to that in SW-D2 around sunrise (Fig. 16a). However, between

07:30 and 09:30 LST, 3 and 5 h after sunrise, this difference in SW-D5 becomes larger than that in SW-D2 as the difference in decoupling between SW-D5 and SW-D2 becomes larger; the decoupling difference increases, as the solar-radiation difference between SW-D5 and SW-D2 increases with time after sunrise. With less decoupling in SW-D5, the feedbacks between increased CDNC and decreased supersaturation with increased aerosols, which is already set up before near sunrise, get reinforced more by the water-vapor flux into the cloud layer than those in SW-D2 as time progresses after sunrise. In other words, the more efficient transport of the water-vapor flux into the cloud layer with less decoupling around sunrise (as shown in the comparison of Fig. 16a and b) provides more water vapor for the feedbacks between increased CDNC and decreased supersaturation at high aerosol in SW-D5 than in SW-D2. This leads to larger increases in CDNC with smaller decreases in supersaturation at high aerosol in SW-D5 than in SW-D2 around sunrise. Then, larger increased feedbacks between increased CDNC and decreased supersaturation induces more increased updrafts and this increases the transport of water vapor more, setting up stronger feedbacks among CDNC, supersaturaion, and water-vapor flux at high aerosol in SW-D5 than in SW-D2. Hence, the sub-cloud water-vapor flux, condensation and updrafts increases at high aerosol become larger in SW-D5 than in SW-D2 as time progresses after sunrise as shown in Figs. 8 and 9 (depicting the time series of condensation and updrafts) and in Figure 16. This leads to the increasing difference in the LWP increase in the high-aerosol case between SW-D5 and SW-D2 with time after sunrise as shown in Fig. 4, which explains most of the time- and domain-averaged difference in the LWP increase in the high-aerosol case between SW-D5 and SW-D2.

6 Summary and conclusion

This study examined the impact of variations in solar radiation on aerosol-cloud interactions in thin stratocumulus clouds with LWP<50 g m^{-2}. For this examination, four sets of simulations of stratocumulus clouds with different downward solar radiation at

the model top were performed; each set of simulations is composed of a high-aerosol run and a low-aerosol run. In the first set of simulations, a case at (42° N, 60° W) off the coast of Maine (CONTROL) is simulated for a PD aerosol case (the high-aerosol run) and a PI aerosol case (the low-aerosol run), respectively. The model-top solar radiation in CONTROL was multiplied by a factor of 1.5 to the first set of simulations (SW-M1.5). The CONTROL solar radiation, divided by a factor of 2 and 5, was applied to the second (SW-D2) and third (SW-D5) of sets, respectively.

As decoupling in the MBL increased with increasing solar radiation, the transport of water vapor from the surface to cloud layer became less efficient, leading to less condensation. This led to a decrease in the LWC and thus LWP with increasing solar radiation, since condensation controlled the LWC and thus the LWP, and the role of sedimentation and the conversion of cloud liquid to rain (autoconversion+ collection of cloud liquid by rain) in the determination of the LWP was negligible in the thin clouds simulated here. Smaller LWC with larger solar radiation provided a smaller source for rain formation through the conversion of cloud liquid to rain and this led to a decrease in surface precipitation with increasing solar radiation in SW-D2 and SW-D5 and to no surface precipitation in CONTROL and SW-M1.5.

Whether or not the surface precipitation was present determined how increasing aerosols interacted with clouds. In SW-D2 and SW-D5 with surface precipitation, interactions among CDNC, supersaturation, and updrafts determined the LWP response to aerosols, while these interactions established feedbacks with interactions between rain evaporation and cloud-base instability in CONTROL and SW-M1.5 with no surface precipitation. With the increased decoupling in SW-D2 and SW-D5, the interactions among CDNC, supersaturation, and updrafts decreased due to the decreasing transport of water vapor to the cloud layer. This led to the smaller condensation and LWPs in each of the high-aerosol run and the low-aerosol run in SW-D2 than in SW-D5. With the increase in the decoupling as time progresses after sunrise, the difference in the water-vapor flux between the high-aerosol run and the low-aerosol run became larger in both SW-D2 and SW-D5. It was notable that the increase in the difference in

ACPD
9, 23791–23833, 2009

water-vapor flux was larger in SW-D5 than in SW-D2. This led to more increased interactions among CDNC, supersaturaton, and updrafts at high aerosol as compared to those at low aerosol in SW-D5 than in SW-D2. Thus, the LWP increase at high aerosol was larger in SW-D5 than in SW-D2. In CONTROL and SW-M1.5 with no surface precipitation, rain evaporates mostly around cloud base. Due to the larger conversion of cloud liquid to rain, more rain evaporates around cloud base, leading to the larger cloud-base instability at low aerosol than at high aerosol. This increased instability was larger than the decreased interactions among CDNC, supersaturation, and updrafts at low aerosol, leading to the increased LWP at low aerosol than at high aerosol in these cases with no surface precipitation. The increase in the cloud-base instability was affected by solar radiation and thus decoupling. As solar radiation increased, the increase in rain evaporation at low aerosol decreased, leading to smaller increases in the cloud-base instability at low aerosol in SW-M1.5 than in CONTROL. Thus, the LWP increase at low aerosol was smaller in SW-M1.5 than in CONTROL.

In this study, identical surface fluxes from observations were prescribed for all of simulations. Therefore, surface fluxes did not contribute to the different instability and feedbacks among CDNC, condensation and dynamics. We focused on the effect of aerosols on thin clouds and its dependence on solar radiation for an identical net heat and moisture supplied to or removed from the domain by the large-scale flow and surface fluxes. Although feedbacks from differences in clouds onto the large-scale flow and surface fluxes cannot be captured by this design, this isolates the interactions among aerosols, microphysics, local dynamics and instability and enables the identification of microphysics-aerosol interactions on the scale of cloud systems.

It is hard to say whether the variation of solar radiation which accompanies the change of season or latitude will significantly impact the effect of aerosols on thin clouds, since the varying solar radiation will change the environmental factors such as surface fluxes which are known to affect aerosol-cloud interactions (Guo et al., 2007). It is likely that these fluxes increase with an increase in the solar radiation, since increasing solar radiation generally increases the surface temperature and, thus,

humidity. As shown in Lee and Penner (2009) and Guo et al. (2007), an increase in the surface fluxes tends to increase condensation and LWP and, thus, to counter the effect of the increasing solar radiation on thin clouds. Hence, the effect of solar radiation on the effect of aerosols on thin clouds in reality may not be as strong as that shown here. Nevertheless, this study showed that a variation in solar radiation could induce changes in the in-cloud and cloud-base feedbacks which control the response of thin clouds to aerosols. This indicates that solar radiation needs to be included in the sets of environmental conditions which can affect aerosol-cloud interactions in thin clouds. Generally, the humidity, large-scale subsidence, sea surface temperature, and surface sensible and latent heat fluxes are intensely studied as important factors which control aerosol-cloud interactions in stratocumulus clouds (Jiang et al., 2002; Ackerman et al., 2004; Guo et al., 2007). It is open to future study to show how the effect of solar radiation on thin clouds interacts with these other environmental factors. Roughly 28% of the globe is covered by thin clouds, and the radiative fluxes at the Earth's surface and top of atmosphere are very sensitive to the LWP variation when the LWP becomes smaller than $\sim 50\,\mathrm{g\,m^{-2}}$ (Turner et al., 2007; McFarlane and Evans, 2004; Shupe and Interieri, 2004; Marchand et al., 2003). Hence, a more understanding of the effect of interactions among solar radiation and other environmental factors on aerosol-cloud interactions in thin clouds is critical to the correct assessment of the AIE.

Acknowledgements. The authors wish to thank Derek Posselt and Wei-Kuo Tao for providing the GCE coupled with double-moment microphysics used here and valuable discussions. This paper was prepared under US Department of Energy ARM program (DE FG02 97 ER62370).

References

Abdul-Razzak, H. and Ghan, S. J.: A parameterization of aerosol activation – 2. Multiple aerosol types, J. Geophys. Res., 105, 6837–6844, 2000.

Abdul-Razzak, H. and Ghan, S. J.: A parameterization of aerosol activation – 3. Sectional representation, J. Geophys. Res., 107, D34026, doi:10.1029/2001JD000483, 2002.

Ackerman, A. S., Kirkpatrick, M. P., Stevens, D. E., and Toon, O. B.: The impact of humidity above stratiform clouds on indirect aerosol climate forcing, Nature, 432, 1014–1017, 2004.

Albrecht, B. A.: Aerosols, cloud microphysics, and fractional cloudiness, Science, 245, 1227–1230, 1989.

Bretherton, C. S. and Wyant, M. C.: Moisture transport, lower-tropospheric stability, and decoupling of cloud-topped boundary layers, J. Atmos. Sci., 54, 148–167, 1997.

Chuang, C. C., Penner, J. E., Taylor, K. E., Grossman, A. S., and Walton, J. J.: An assessment of the radiative effects of anthropogenic sulfate, J. Geophys. Res., 102, 3761–3778, 1997.

Cotton, W. R., Stephens, M. A., Nehrkorn, T., and Tripoli, G. J.: The Colorado State University three-dimensional cloud/mesoscale model, Part II: An ice phase parameterization, J. Rech. Atmos. 16, 295–319, 1982.

Donner, L. J., Seman, C. J., and Hemler, R. S.: Three-dimensional cloud-system modeling of GATE convection, J. Atmos. Sci., 56, 1885–1912, 1999.

Feingold, G., Stevens, B., Cotton, W. R., and Frisch, A. S.: The relationship between drop in-cloud residence time and drizzle production in numerically simulated stratocumulus clouds, J. Atmos. Sci., 53, 1108–1122, 1996.

Feingold, G., Tzivion, S., and Levin, Z.: Evolution of raindrop spectra, Part I: Solution to the stochastic collection/breakup equation using the method of moments, J. Atmos. Sci., 45, 3387–3399, 1988.

Grabowski, W. W., Wu, X., Moncrieff, M. W.: Cloud resolving modeling of tropical cloud systems during phase III of GATE, Part I: Two-Dimensional Experiments, J. Atmos. Sci., 53, 3684–3709, 1996.

Guo, H., Penner, J. E., Herzog, M., and Xie, S.: Investigation of the first and second aerosol indirect effects using data from the May 2003 Intensive Operational Period at the Southern Great Plains, J. Geophys. Res., 112, D15206, doi:10.1029/2006JD007173, 2007.

Jiang, H., Feingold, G., and Cotton, W. R.: Simulations of aerosol-cloud-dynamical feedbacks resulting from entrainment of aerosol into the marine boundary layer

during the Atlantic Stratocumulus Transition Experiment, J. Geophys. Res., 107, 4813, doi:10.1029/2001JD001502, 2002.
Krueger, S. K., Cederwall, R. T., Xie, S. C., and Yio, J. J.: GCSS Working Group for Model Intercomparison – Procedures for Case 3: Summer 1997 ARM SCM IOP, Technical report obtainable from ftp://ftp.met.utah.edu/pub/skrueger/gcss_wg4_case3/gcss-wg4-case3-doc.pdf, 1999.
Lee, S. S. and Penner, J. E.: Factors determining the effect of aerosols on cloud mass and the dependence of these factors on liquid-water path, Atmos. Chem. Phys. Discuss., 9, 19313–19350, 2009, http://www.atmos-chem-phys-discuss.net/9/19313/2009/.
Lee, S. S., Penner, J. E., and Saleeby, S. M.: Aerosol effects on liquid-water path of thin stratocumulus clouds, J. Geophys. Res., 114, D07204, doi:10.1029/2008JD010513, 2009.
Liu, X. H., Penner, J. E., and Herzog, M.: Global modeling of aerosol dynamics: Model description, evaluation, and interactions between sulfate and nonsulfate aerosols, J. Geophys. Res., 110, D18206, doi:10.1029/2004JD005674, 2005.
Marchand, R., Ackerman, T., Westwater, E. R., Clough, S. A., Cady-Pereira, K., and Liljegren, J. C. :An assessment of microwave absorption models and retrievals of cloud liquid water using clear-sky data, J. Geophys. Res., 108, 4773, doi:10.1029/2003JD003843, 2003.
McFarlane, S. A. and Evans, K. F.: Clouds and shortwave fluxes at Nauru, Part I: Retrieved cloud properties, J. Atmos. Sci., 61, 733–744, 2004.
Paluch, I. R. and Lenschow, D. H.: Stratiform cloud formation in the marine boundary layer, J. Atmos. Sci., 48, 2141–2158, 1991.
Penner, J. E., Andreae, M., Annegarn, H., et al.: Report to intergovernmental panel on climate change from the scientific assessment working group (WGI), in: Climate Change 2001: The Scientific Basis, chap. 5, edited by: J. T. Houghton, B. Nyenzi, and J. Prospero, Cambridge University Press, New York, 289-348, 2001.
Pruppacher, H. R. and Klett, J. D.: Microphysics of Clouds and Precipitation, D. Reidel, 714 pp., 1978.
Rogers, R. R. and Yau, M. K.: A short course in cloud physics, Pergamon Press, 293 pp., 1991.
Saleeby, S. M. and Cotton, W. R.: A large-droplet mode and prognostic number concentration of cloud droplets in the Colorado state university regional atmospheric modeling system (RAMS), Part I: Module description and supercell test simulations, J. Appl. Meteorol., 43, 182–195, 2004.

Shupe, M. D. and Intrieri, J. M.: Cloud radiative forcing of the Arctic surface: The influence of cloud properties, surface albedo, and solar zenith angle, J. Climate, 17, 616–628, 2004.
Simpson, J. and Tao, W.-K.: The Goddard Cumulus Ensemble model, Part II: Applications for studying cloud precipitating processes and for NASA TRMM, Terr. Atmos. Ocean. Sci., 4, 73–116, 1993.
Tao, W.-K., Simpson, J., Baker, D., et al.: Microphysics, radiation and surface processes in the Goddard Cumulus Ensemble (GCE) model, Meteorol. Atmos. Phys., 82, 97–137, 2003.
Tao, W.-K. and Simpson, J.: The Goddard Cumulus Ensemble model, Part I: Model description, Terr. Atmos. Ocean. Sci., 4, 19–54, 1993.
Turner, D. D., Vogelmann, A. M., Austin, R. T., et al.: Thin liquid water clouds: Their importance and our challenge, B. Am. Meteorol. Soc., 88, 177–190, 2007.
Twomey, S.: The influence of pollution on the shortwave albedo of clouds, J. Atmos. Sci., 34, 1149–1152, 1977.
Twomey, S.: Pollution and the Plantetary Albedo, Atmos. Environ., 8, 1251–1256, 1974.
Rogers, R. R. and Yau, M. K.: A short course in cloud physics, Pergamon Press, 293 pp., 1991.
Wang, M., Penner, J. E., and Liu, X.: Coupled IMPACT aerosol and NCAR CAM3 model: Evaluation of predicted aerosol number and size distribution, J. Geophys. Res., 114, D06302, doi:10.1029/2008JD010459, 2009.
Xu, K.-M., Cederwall, R. T., Donner, L. J., et al.: An intercomparison of cloud-resolving models with the Atmospheric Radiation Measurement summer 1997 Intensive Observation Period data, Q. J. Roy. Meteorol. Soc., 128, 593–624, 2002.

Table 1. Summary of simulations.

Simulations		Background aerosols	Downward model top SW	Time-averaged model top (at 0.01 hPa) SW ($W\,m^{-2}$)
CONTROL	High-aerosol run	PD aerosol	SW flux at (30° N, 123° W) on 1 July	1139
	Low-aerosol run	PI aerosol	Same as in the high-aerosol run in CONTROL	1139
SW-M1.5	High-aerosol run	PD aerosol	Same as in the high-aerosol run in CONTROL but increased by a factor of 1.5	1709
	Low-aerosol run	PI aerosol	Same as in the high-aerosol run in CONTROL but increased by a factor of 1.5	1709
SW-D2	High-aerosol run	PD aerosol	Same as in the high-aerosol run in CONTROL but reduced by a factor of 2	570
	Low-aerosol run	PI aerosol	Same as in the high-aerosol run in CONTROL but reduced by a factor of 2	570
SW-D5	High-aerosol run	PD aerosol	Same as in the high-aerosol run in CONTROL but reduced by a factor of 5	228
	Low-aerosol run	PI aerosol	Same as in the high-aerosol run in CONTROL but reduced by a factor of 5	228

ACPD

9, 23791–23833, 2009

Table 2. Domain-averaged LWP, upward model top SW, precipitation rate, budget terms of cloud liquid (i.e. condensation, evaporation, and the conversion), sedimentation, the ratio of conversion to condensation and of sedimentation to condensation.

	SW-M1.5			CONTROL			SW-D2			SW-D5		
	High aerosol	Low aerosol	High minus Low	High aerosol	Low aerosol	High minus Low	High aerosol	Low aerosol	High minus Low	High aerosol	Low aerosol	High minus Low
LWP ($g\,m^{-2}$)	11.3	13.1	−1.8	13.4	17.1	−3.7	26.6	24.0	2.6	38.2	31.3	6.9
Upward model top SW ($W\,m^{-2}$)	170.9	173.1	−2.2	138.2	142.3	−4.1	85.6	80.1	4.5	52.4	43.2	9.2
Precipitation rate (mm day^{-1})	0.00	0.00	0.00	0.00	0.00	0.00	0.03	0.05	−0.02	0.04	0.07	−0.03
$<Q_{cond}>$ Condensation (mm)	0.24	0.26	−0.02	0.32	0.34	−0.02	0.65	0.58	0.07	0.95	0.78	0.17
$<Q_{evap}>$ Evaporation (mm)	0.23	0.25	−0.02	0.31	0.32	−0.01	0.59	0.51	0.08	0.83	0.66	0.17
$<Q_{auto}>$ Autoconversion of cloud liquid to rain + $<Q_{accr}>$ Accretion of cloud liquid by rain (mm)	0.003	0.004	−0.001	0.004	0.009	−0.005	0.031	0.043	−0.012	0.063	0.085	−0.022
$<\|Q_{sed}\|>$ In-cloud sedimentation (mm)	0.006	0.008	−0.002	0.009	0.011	−0.002	0.050	0.055	−0.005	0.112	0.141	−0.029
$(<Q_{auto}>+<Q_{accr}>)/<Q_{cond}>$ Conversion efficiency	0.01	0.02	−0.01	0.01	0.03	−0.02	0.05	0.07	−0.02	0.07	0.11	−0.04
$<\|Q_{sed}\|>/<Q_{cond}>$	0.03	0.03	0.00	0.03	0.03	0.00	0.08	0.10	−0.02	0.12	0.18	−0.06

ACPD
9, 23791–23833, 2009

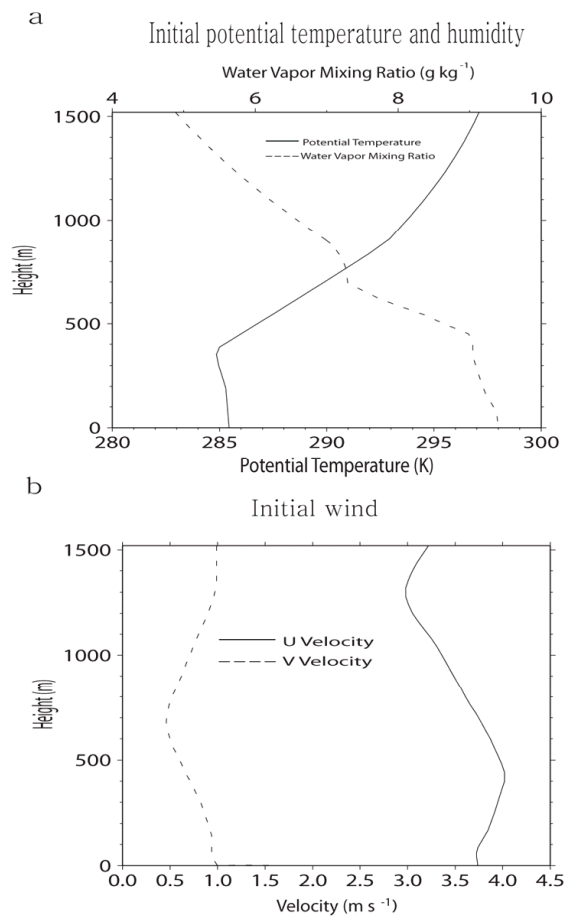

Fig. 1. Vertical profiles of **(a)** initial potential temperature and water vapor mixing ratio and **(b)** initial horizontal wind (u, v) velocity.

ACPD
9, 23791–23833, 2009

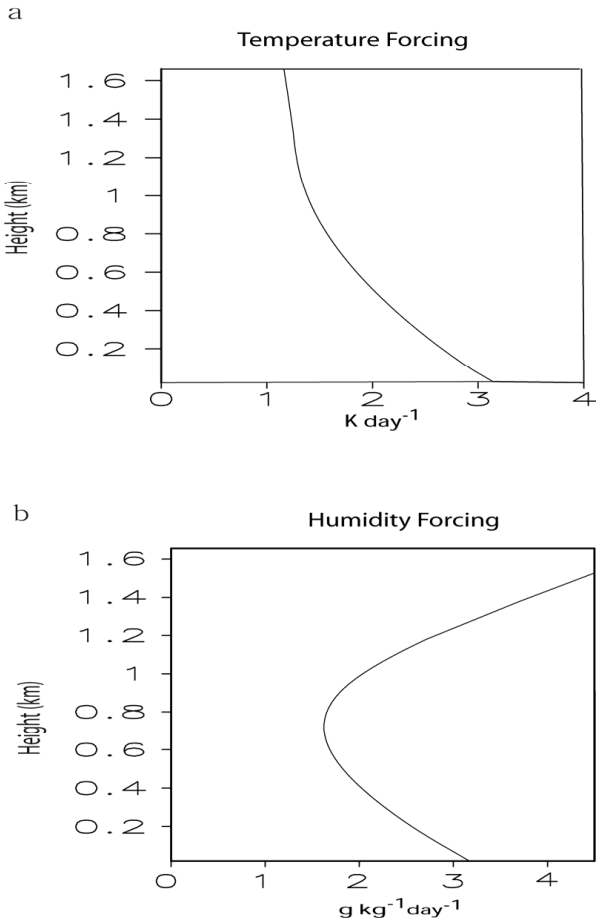

Fig. 2. Vertical distribution of the time- and area-averaged **(a)** potential temperature large-scale forcing (K day^{-1}) and **(b)** humidity large-scale forcing (g kg^{-1} day^{-1}).

ACPD
9, 23791–23833, 2009

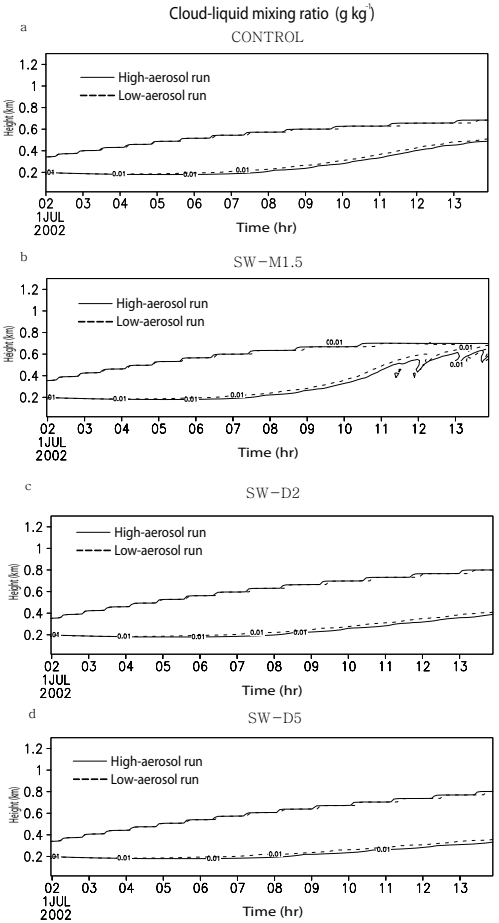

Fig. 3. Time-height cross section of cloud-liquid mixing ratio ($g\,kg^{-1}$). Contours are at $0.01\,g\,kg^{-1}$.

ACPD
9, 23791–23833, 2009

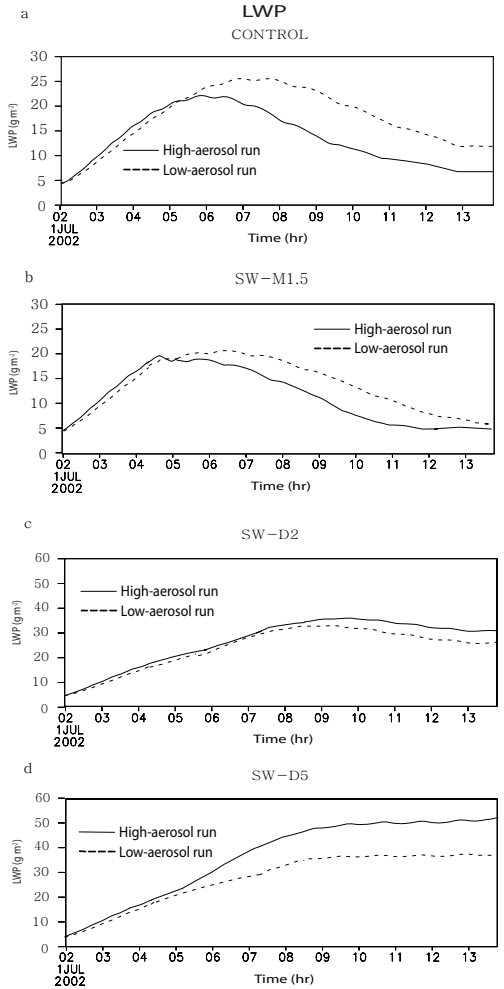

Fig. 4. Time series of LWP ($g\,m^{-3}$) averaged over the horizontal domain.

ACPD
9, 23791–23833, 2009

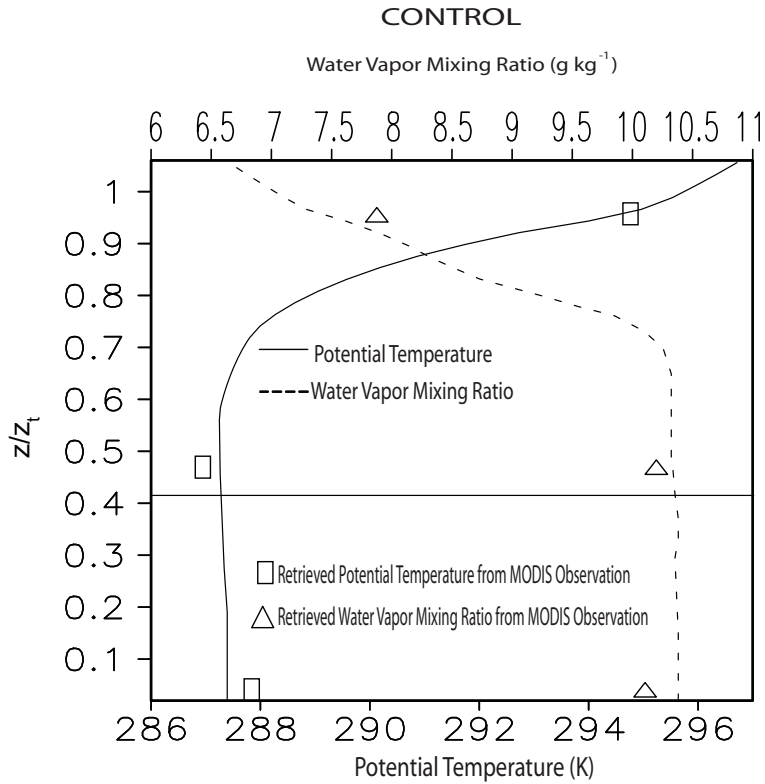

Fig. 5. Vertical distribution of time- and area-averaged potential temperature and water vapor mixing ratio in the high-aerosol run for CONTROL. Squares (triangles) represent the retrieved potential temperature (water-vapor mixing ratio) from the MODIS observation. The solid horizontal line is the average cloud-base height normalized with respect to cloud-top height (z_t).

ACPD
9, 23791–23833, 2009

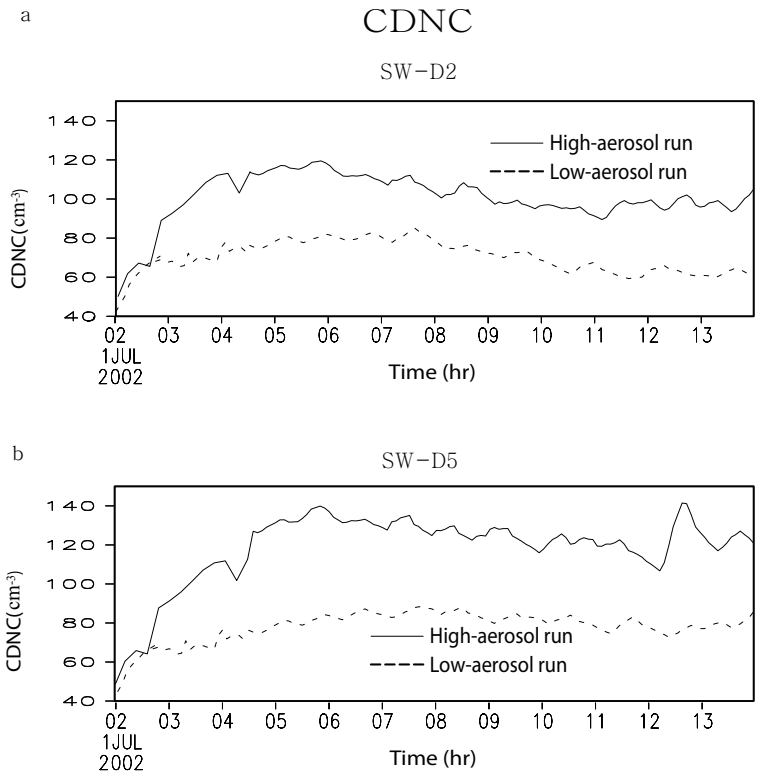

Fig. 6. Time series of the conditionally averaged CDNC for SW-D2 and SW-D5. For the conditional average, the grid points with positive values of condensation are collected and the other grid points are excluded. The conditional average is the arithmetic mean of a variable of interest (here, CDNC) over these collected grid points.

ACPD
9, 23791–23833, 2009

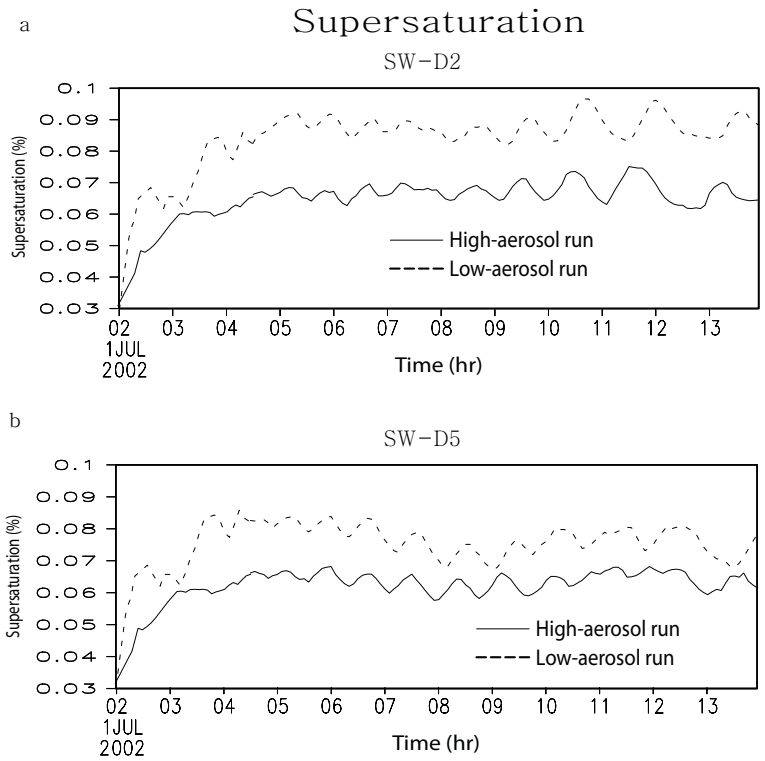

Fig. 7. Time series of conditionally averaged supersaturation for SW-D2 and SW-D5. The conditional average is the arithmetic mean of a variable of interest (here, supersaturation) over collected grid points with non-zero condensation.

ACPD
9, 23791–23833, 2009

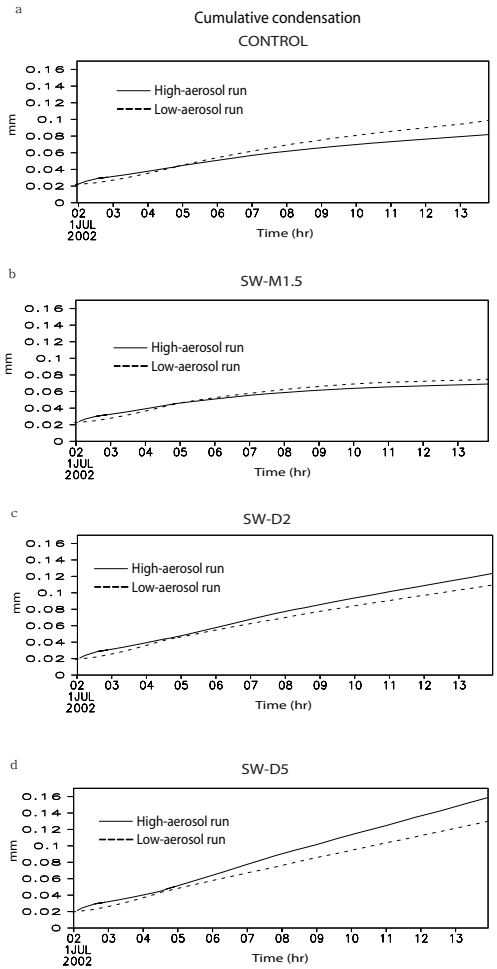

Fig. 8. Time series of cumulative condensation (mm) averaged over the horizontal domain.

ACPD
9, 23791–23833, 2009

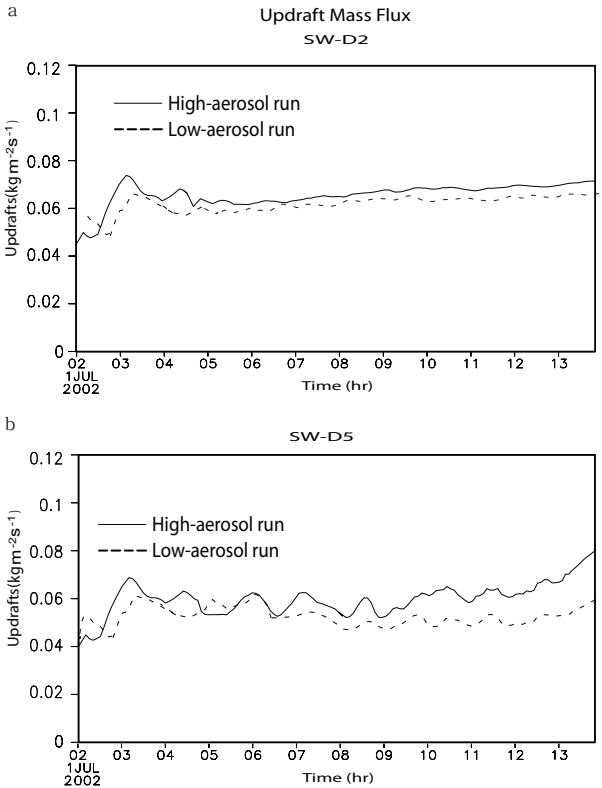

Fig. 9. Time series of domain-averaged updraft mass flux ($kg\,m^{-2}\,s^{-1}$) for SW-D2 and SW-D5.

ACPD
9, 23791–23833, 2009

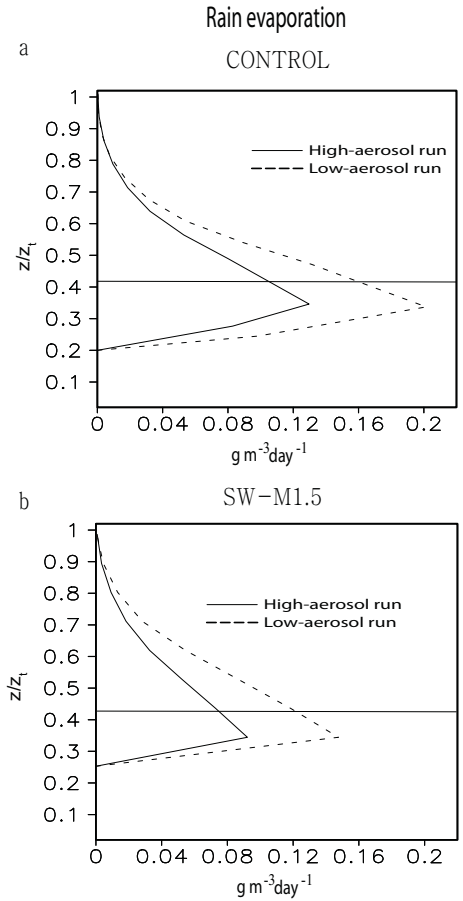

Fig. 10. Vertical distribution of time- and area-averaged rain evaporation over the entire simulation period for CONTROL and SW-M1.5. The solid horizontal line in each figure is the average cloud-base height normalized with respect to cloud-top height (z_t).

ACPD
9, 23791–23833, 2009

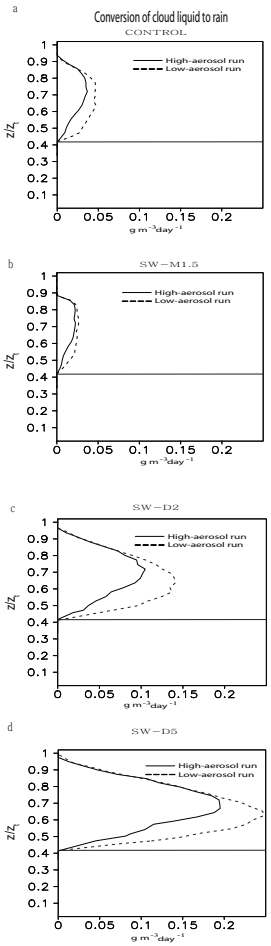

Fig. 11. Vertical distribution of time- and area-averaged conversion of cloud liquid to rain in $g\,m^{-3}\,day^{-1}$. The solid horizontal line in each figure is the average cloud-base height normalized with respect to cloud-top height (z_t).

ACPD
9, 23791–23833, 2009

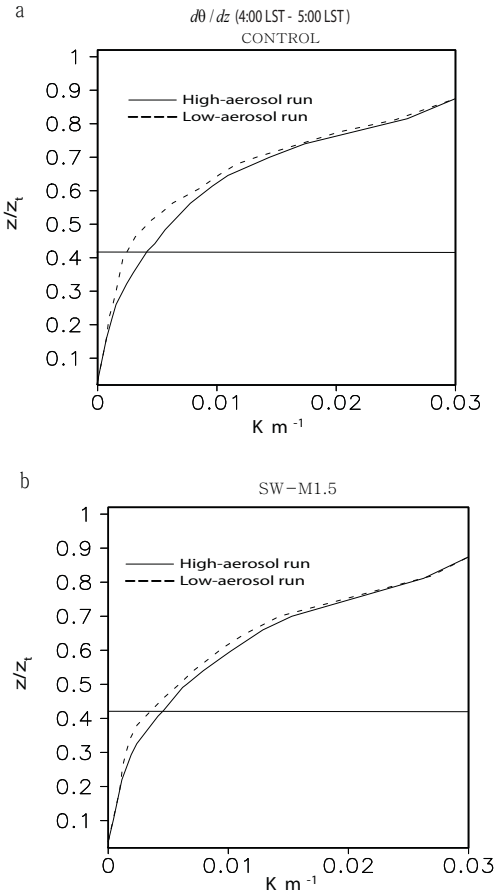

Fig. 12. Vertical distribution of time- and area-averaged $\frac{d\theta}{dz}$ ($\mathrm{K\,m^{-1}}$) over the period between 04:00 LST and 05:00 LST for CONTROL and SW-M1.5. The solid horizontal line in each figure is the average cloud-base height normalized with respect to cloud-top height (z_t).

ACPD
9, 23791–23833, 2009

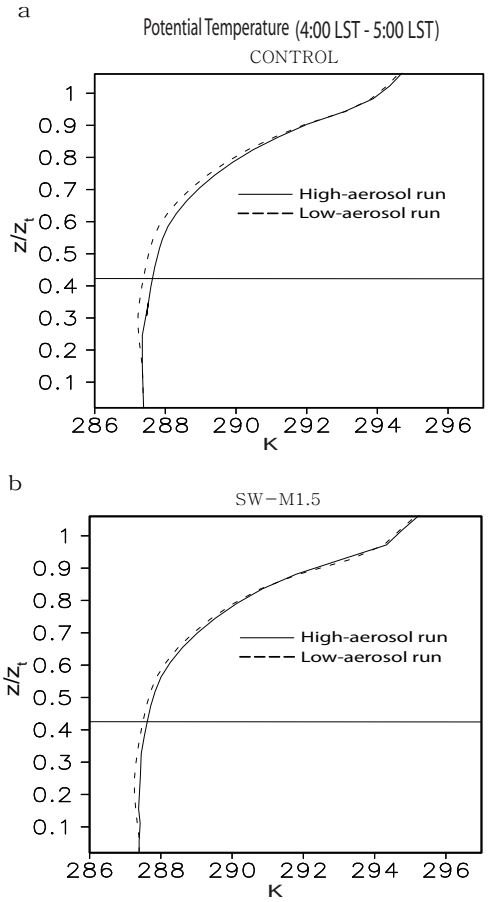

Fig. 13. Vertical distribution of time- and area-averaged θ (K) over the period between 04:00 LST and 05:00 LST for CONTROL and SW-M1.5. The solid horizontal line in each figure is the average cloud-base height normalized with respect to cloud-top height (z_t).

ACPD
9, 23791–23833, 2009

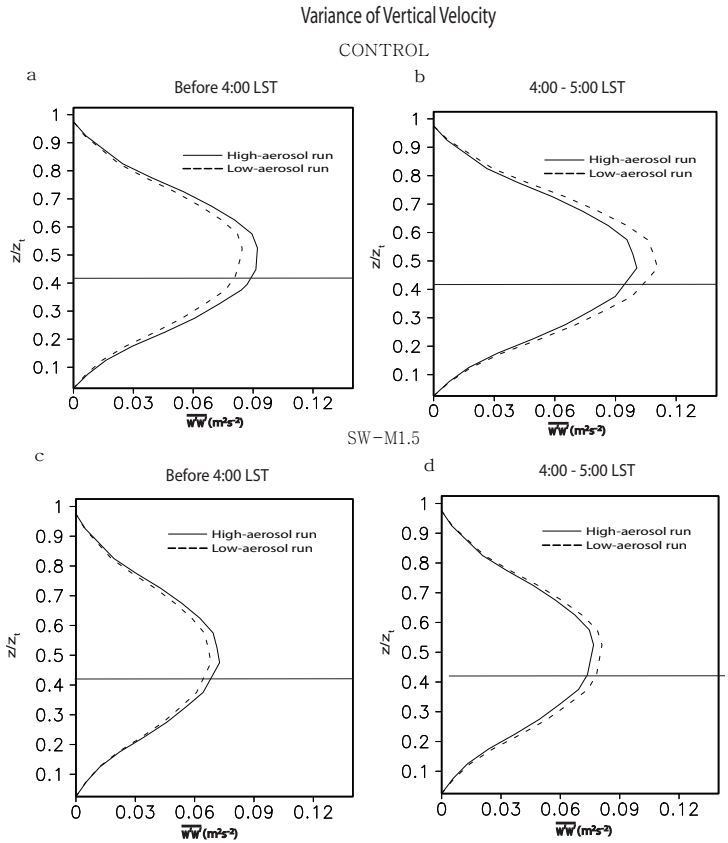

Fig. 14. Vertical distribution of the time- and area-averaged variance of vertical velocity ($\overline{w'w'}$) ($m^{-2}\,s^{-2}$) for CONTROL and SW-M1.5. **(a)** and **(c)** are averaged over the period before 04:00 LST and **(b)** and **(d)** are averaged over the period between 04:00 LST and 05:00 LST. The solid horizontal line in each figure is the average cloud-base height normalized with respect to cloud-top height (z_t).

ACPD
9, 23791–23833, 2009

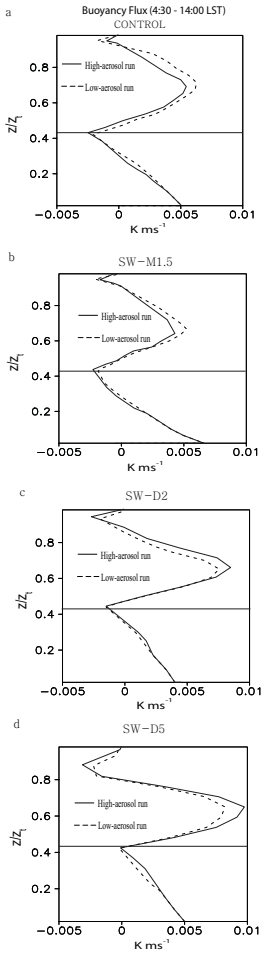

Fig. 15. Vertical distribution of the time- and area-averaged buoyancy flux ($\overline{w'\theta_v'}$) over the period between 04:30 LST and 14:00 LST. The solid horizontal line in each figure is the average cloud-base height normalized with respect to cloud-top height (z_t).

ACPD
9, 23791–23833, 2009

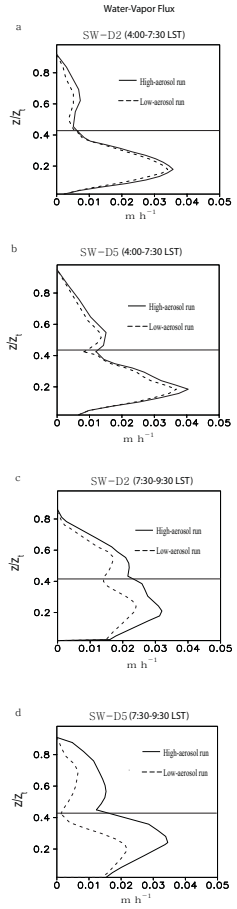

Fig. 16. Vertical distribution of the time- and area-averaged water-vapor flux ($\overline{w'q'_v}$) in m h^{-1} for SW-D2 and SW-D5. **(a)** and **(b)** are averaged over the period between 04:00 LST and 07:30 LST and **(c)** and **(d)** are averaged over the period between 07:30 LST and 09:30 LST. The solid horizontal line in each figure is the average cloud-base height normalized with respect to cloud-top height (z_t).

ACPD
9, 23791–23833, 2009